PCCP

Accepted Manuscript

This is an *Accepted Manuscript*, which has been through the Royal Society of Chemistry peer review process and has been accepted for publication.

Accepted Manuscripts are published online shortly after acceptance, before technical editing, formatting and proof reading. Using this free service, authors can make their results available to the community, in citable form, before we publish the edited article. We will replace this *Accepted Manuscript* with the edited and formatted *Advance Article* as soon as it is available.

You can find more information about *Accepted Manuscripts* in the Information for Authors.

Please note that technical editing may introduce minor changes to the text and/or graphics, which may alter content. The journal's standard Terms & Conditions and the Ethical guidelines still apply. In no event shall the Royal Society of Chemistry be held responsible for any errors or omissions in this *Accepted Manuscript* or any consequences arising from the use of any information it contains.

ROYAL SOCIETY OF CHEMISTRY

www.rsc.org/pccp

Physical Chemistry Chemical Physics
CREATED USING THE RSC LaTeX PCCP ARTICLE TEMPLATE – SEE www.rsc.org/electronicfiles FOR DETAILS
ARTICLE TYPE www. rsc.org/xxxxxx | XXXXXXXX

Atomistic Simulations of TeO_2-based Glasses: Interatomic Potentials and Molecular Dynamics

Anastasia Gulenko, Olivier Masson,* Abid Berghout, David Hamani and Philippe Thomas

Received Xth XXXXXXXXXX 20XX, Accepted Xth XXXXXXXXX 20XX
First published on the web Xth XXXXXXXXXX 200X
DOI: 10.1039/b000000x

In this work we present for the first time empirical interatomic potentials able to reproduce TeO_2-based systems. Using these potentials in classical molecular dynamics simulations, we obtained first results on the pure TeO_2 glass structure model. Calculated pair distribution function is in a good agreement with the experimental one, which indicates a realistic glass structure model. We investigated the short- and medium-range TeO_2 glass structure. The local environment of Te atom strongly varies, so that the glass structure model has a broad Q^n_m polyhedra distribution. The glass network is described as weakly connected and with a large number of terminal oxygen atoms.

1 Introduction

Tellurium oxide-based glasses are among the most promising candidates for integration in non-linear optical devices, such as up-conversion frequency systems and high speed optical-switches, since they exhibit high linear and nonlinear optical properties. In particular their susceptibilities $\chi^{(3)}$ are the highest among the known oxide glasses, 50–100 times higher than that of glassy SiO_2 [1]. The origin of these properties, which is of great interest for material science, has been early attributed to the electronic ($5s^2$) lone pair (LP) of tellurium (IV) atoms when bonded to oxygen atoms [2]. Recent works however suggest that the structure of the glass itself and in particular the nature of the Te–O–Te bridges [3–5] is responsible to a large extend for these particular features. A better understanding of the origin of non-linear optical properties thus requires a better knowledge of the glass structure.

The structure of modified TeO_2-glasses has been relatively well investigated by different techniques: Infrared (IR) and Raman spectroscopy [6,7], Magic Angle Spinning (MAS)–Nuclear Magnetic Resonance (NMR) [8,9], NMR, Neutron and X-ray diffraction combined with Reverse Monte Carlo (RMC) simulations [10–13]. These studies describe the tellurite glasses as complex systems composed of various TeO_x structural units with either bridging oxygen (BO) atoms or non bridging oxygen (NBO) atoms. These units are described in terms of Q^n_m units, where m is the total number of BO and NBO (within a chosen R_{cutoff}) atoms and n is the number of BO atoms. More precisely, the authors in [10,11] established that the presence of five tellurite polyhedra (Q^0_3, Q^1_3, Q^2_3, Q^3_4, Q^4_4, see Fig. 1) in the glass model is necessary to achieve a good agreement between experimental data and RMC model of modified TeO_2 glasses. All these Q^n_m polyhedra are found in modified tellurite crystals, whereas the pure TeO_2 polymorphs (α-, β- and γ-TeO_2) consist of only Q^4_4 and Q^4_{3+1} † units [14–17]. This is the tellurium (IV) electronic LP steric effect that produces the strong asymmetry in oxygen atoms distribution in Te atom environment (Fig. 1).

The studies of pure amorphous TeO_2 system are represented with only two works in the literature to date. The first one is an *ab initio* molecular dynamics (MD) studies by Pietrucci *et al.* [18]. These authors report a glass model that consists of various Q^n_m units like those determined by RMC modelling, but also of other Q^3_3 and Q^5_5 units, and Q^3_3 units make up an important contribution (20.4 %) in Q^n_m population. Also the authors report the presence of 14% of terminal oxygen atoms, which does not fit well with the continuous glass network model of Zachariasen [19]. The second work on pure amorphous TeO_2 system by Barney *et al.* [20] is based on recent neutron diffraction experiment . These authors made the precise measurements of tellurium coordination number n_{TeO} and obtained a value 3.68(4), that implies that the glass structure is formed from about 2/3 four-coordinated units and 1/3 three-coordinated units, that gives, in turn, about 16% of terminal oxygen atoms. Further they propose a simple connectivity model for the glass, where TeO_3 and TeO_4 units in ratio 1 : 2 form the rings like in crystalline $K_2Te_4O_9$ structure. This especially high concentration of NBO atoms can explain the particular behaviour of TeO_2 as glass former. TeO_2 is known as a conditional glass former and requires fast-quenching tech-

Laboratoire Science des Procédés Céramiques et de Traitements de Surface (SPCTS) UMR 7315 CNRS
Université de Limoges, Faculté des Sciences et Techniques, 12 rue Atlantis, 87068 LIMOGES Cedex, FRANCE; E-mail: olivier.masson@unilim.fr

† This notation stands for TeO_x unit with three short (< 2.02 Å) Te–O bonds and one elongated (2.2 Å) bond in γ-TeO_2

Physical Chemistry Chemical Physics Accepted Manuscript

niques to form a glass. The resulting amorphous material is not stable to devitrification, but could be stabilised by adding, for example, alkali oxides. This is contrary to classical glass formers such as SiO_2, P_2O_5 and B_2O_3, where the modifiers usually break the glass network. Thus, it was proposed in [20] that the facile accommodation of modifier atoms is fairly connected to the presence of a large number of NBO atoms.

These results are highly unusual and require deeper understanding. However, *ab initio* MD methods are limited in size of simulated system and simulation time. The glass model in [18] consisted of only 32 TeO_2 units and was obtained as a result of 16 ps cooling the liquid at a rate of $\approx 10^{14}$ K/s. The authors themselves consider that such a high concentration of NBO atoms might be due to a too high cooling rate used in *ab initio* MD simulation. In other words, the system might have not reached a fully equilibrated glass structure and resembles more to a frozen liquid.

On the contrary, classical MD allows bigger size-scale and longer time-scale simulations in comparison with *ab initio* MD. To our knowledge the classical MD simulations of pure TeO_2 glass have never been presented in the literature because of the absence of established interatomic potentials (IAPs) for TeO_2 system. Classical MD requires very accurate IAPs in order to produce realistic structure model. The only work reported the classical MD simulations for TeO_2-based systems is for ZnO–TeO_2 glasses [21]. The authors used the three-body IAP for Te–O interaction, which could have prevented them to reproduce all the variety of TeO_x structural units by fixing the minimum of potential energy at a certain angle value. In addition, the envelope of the resulting pair distribution function (PDF) does not fit very well the experimental data in medium-range order (3–6 Å).

In this work we report for the first time the IAPs of able to reproduce TeO_2-based systems. We report also the first results of their application to the classical MD simulations for pure TeO_2 glass. The paper is organised as follows. Firstly, we consider the methodology of IAPs derivation in Sec. 2 and their validation in Sec. 3. Then we briefly discuss the MD simulation computational details in Sec. 4 and pass on to the results (Sec. 6). The last section is dedicated to the discussion of the MD glass structure model.

2 Derivation of the Interatomic Potentials

The IAPs were developed in the framework of the Born model of ionic solids. Simple pairwise potentials were used in order to reproduce the various coordinations of Te atom in different TeO_2-based compounds and the high polarisability of both tellurium and oxygen atoms was taken into account by using the core-shell model [22].

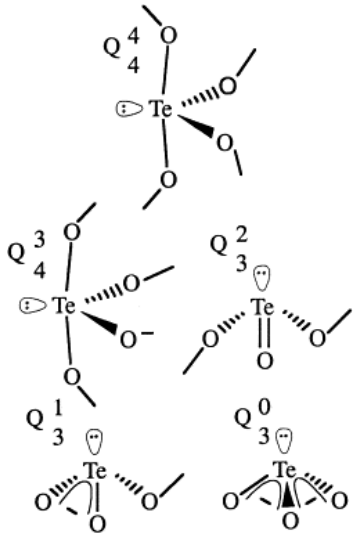

Fig. 1 Structural units Q_m^n found in tellurite crystals, where m is the number of bonded oxygen atoms and n is the number of bridging oxygen atoms. Taken from [10]

2.1 Potential form

In general, the IAP between ions i and j consists of a short-range term and the long-range Coulombic contribution. As the Buckingham potential model has previously proved to be successful in modelling a variety of materials [23,24], it was chosen for this work for the short-range term. Thus, the total force field has a form

$$U_{ij}(r) = A_{ij}e^{-r/\rho_{ij}} - C_{ij}r^{-6} + \frac{q_i q_j}{4\pi\varepsilon_0}\frac{1}{r}, \qquad (1)$$

where A_{ij}, ρ_{ij} and C_{ij} are the Buckingham potential parameters, and q_i is the charge of ion i. In this work we used formal integer charges: +4 for Te and -2 for O.

In the core-shell model the atom is divided into a core and a shell, where all the atom mass is assigned to the core and the charged massless shell permits to model the atom polarisability. The core and the shell are Coulombically screened from each other, but coupled by a harmonic spring of force constant k_2^{cs} which has a potential form [25]:

$$U_{cs} = \frac{1}{2}k_2^{cs}x^2 \qquad (2)$$

where x is the distance between the core and the shell.

By convention, the short-range forces are specified to act on the shell, while the Coulomb potential acts on both the core and the shell, which is not the case in the present work as we will see later.

Consideration of the structure and crystal chemistry of the parent crystalline compound helps to explain the nature of the

This journal is © The Royal Society of Chemistry [year]

Physical Chemistry Chemical Physics Accepted Manuscript

relevant glass properties. While glasses lack long-range order characteristics of crystals, the chemical forces controlling the short-range order are similar. Therefore, knowledge of local structure in various crystalline compounds can clarify the Te(IV) atom environment in glasses.

The software used to derive IAPs was GULP (General Utility Lattice Program)[26]. Firstly, the empirical fitting procedure was performed that implies determination of potential parameters by reproducing experimental structural data. The experimental crystalline structure is fitted by varying the potential parameters so as to minimise the energy of the configuration. To improve the fit quality we used elastic constants data as second derivative information. For α-TeO_2[27] the experimental elastic constants data were used and for γ-TeO_2 calculated by *ab initio*[28] and lattice dynamics[17] methods.

2.2 Interatomic interactions

We performed IAPs fitting to pure tellurium oxide phases $\alpha-$, $\beta-$ and $\gamma-TeO_2$[14,16,17]. In these polymorphs the Te(IV) atom is found in rather particular environments. In $\alpha-TeO_2$ the coordination polyhedron of Te atoms has the form of a disphenoid TeO_4 (Q_4^4 in Fig. 1), or if we take into account the electronic LP of tellurium atom (E), a distorted trigonal bipyramid TeO_4E with one free equatorial vertex. Two equatorial Te–O bonds are short (1.880 Å) and two axial bonds have intermediate bond length (2.121 Å). If we consider two more distant oxygen atoms with bond lengths Te–O = 2.867 Å, we get a strongly distorted octahedral environment of Te atoms so that $\alpha-TeO_2$ can be thought of as a derived from rutile-type structure.

Firstly, for O–O interaction we used the established IAP from the Catlow library[29]. For Te–O interaction, preliminary tests with rigid ion model gave a rutile-type structure with a perfect octahedron coordination of Te atom in $\alpha-TeO_2$. The conventional application of the core-shell model, *i.e.* when the short-range forces act on the shells, did not lead to a much better representation of Te atom coordination in $\alpha-TeO_2$. Then the interaction between Te and O was set in a quite unusual way: the tellurium atom core (with the charge +6) and the oxygen atom shell interact via Buckingham potential, while the Te shell (with the charge -2) contributes to Coulombic U_{coul} and core-shell U_{cs} energies. This is the first time that short-range forces are applied to the core while using a core-shell model, and such an application allowed us to model the correct oxygen distribution around Te atom. The interaction scheme is represented in Fig. 2.

The subtle differences in Te atom coordination in $\alpha-TeO_2$ and $\gamma-TeO_2$ required the refinement of the Catlow's parameters for O–O atoms interaction. While in α-TeO_2 we find two short and two intermediate Te–O bonds, in γ-TeO_2 Te atom is coordinated with three short-bonded (< 2.02 Å) oxygen

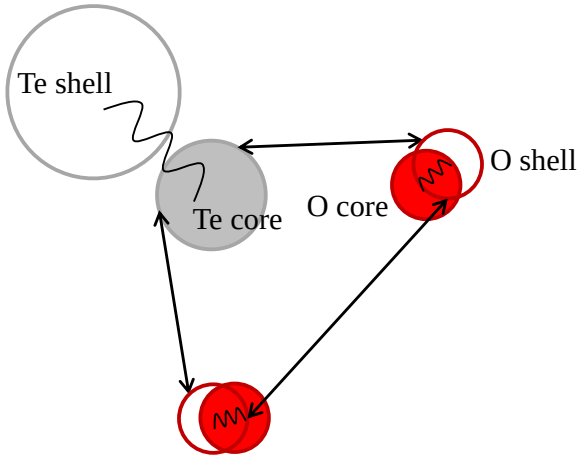

Fig. 2 (Color online) The scheme of considered interactions between atoms in TeO_2 system. The short-range interatomic interactions are indicated with arrows and intra-atomic core-shell interactions are illustrated with springs.

atoms and one oxygen atom with intermediate bond (2.2 Å). The increase of oxygen atom polarisability in O–O interaction permitted to reproduce the TeO_{3+1} unit in $\gamma-TeO_2$.

Besides the pure TeO_2 polymorphs, we investigated a set of TeO_2-based compounds that contain the variety of TeO_x units. The details on this study and on the IAPs derivation procedure can be found elsewhere[30]. Te shell displacements for different structures vary in a large range (from 0.4 Å to 0.72 Å) and affect strongly tellurium atom coordination. In order to satisfy various Te atom coordination, we refined the core-shell model for Te atom by adding an anharmonic term to spring potential of the form:

$$U_{cs} = \frac{1}{2}k_2^{cs}x^2 + \frac{1}{24}k_4^{cs}x^4. \quad (3)$$

This is one more quite unusual feature used in our potential model. Some rare cases of applying an anharmonic spring potential in the core-shell model could be found in[31–34]. The final parameters for IAPs are listed in Table 1.

3 Validation of the Interatomic Potentials

Several tellurium oxides were investigated: M_2TeO_3 (M = Li[35], Na[36], K[37], Cs[38]), $MgTe_2O_5$[39], $\alpha-$[14], $\beta-$[16], $\gamma-TeO_2$[17], $Ag_2Te_4O_{11}$ ($Ag_2Te_2^{IV}Te_2^{VI}O_{11}$)[40], $BaTe_2O_6$ ($BaTe^{IV}Te^{VI}O_6$)[41], $Bi_2Te_4O_{11}$[42], $CaTe_2O_5$[43], $Co_6Te_5O_{16}$[44], $Cs_2Te_4O_{12}$ ($Cs_2Te^{IV}Te_3^{VI}O_{12}$)[45], $K_2Te_4O_{12}$ ($K_2Te^{IV}Te_3^{VI}O_{12}$)[46], $Na_2Te_4O_9$[47], $NiTe_2O_5$[48], $P_2Te_3O_{11}$[49], $SrTe_3O_8$ ($SrTe_2^{IV}Te^{VI}O_8$)[50]. These structures contain a variety of TeO_x

Physical Chemistry Chemical Physics Accepted Manuscript

Table 1 Parameters for Buckingham potential for Te^{4+}–O^{2-} and O^{2-}–O^{2-} interaction and for shell model for both Te and O atoms.

Buckingham potential

	A, eV	ρ, Å	C, eVÅ^6
Te_c^{4+}–O_{sh}^{2-}	1595.266748	0.345867	1.0
O_{sh}^{2-}–O_{sh}^{2-}	82970.688434	0.16099	31.361954

Shell model

	k_2^{cs}, eVÅ^{-2}	k_4^{cs}, eVÅ^{-4}	q_s, e
Te^{4+}	35.736418	90.0	-1.975415
O^{2-}	61.776616	0.0	-3.122581

structural units and most of them are quite asymmetrical.

Among these structures there are $BaTe_2O_6$ and $Cs_2Te_4O_{12}$ with atypical symmetrical environment of Te atom. In $BaTe_2O_6$ structure Te(IV) atom is coordinated to five oxygen atoms, where four of them form a square pyramid with edge of 2.126 Å and the fifth bond is much shorter (1.830 Å). The LP points in the opposite direction of the shortest bond. In $Cs_2Te_4O_{12}$ structure Te(IV) atom is located in the centre of a perfect octahedron TeO_6 formed with six oxygen atoms (distance Te–O = 2,112 Å) and Te LP does not present any stereochemical activity (i.e. the LP is not polarised).

In general, there is a good agreement between calculated and experimental structures considered. The errors in reproducing cell parameters do not exceed 5% and all the varieties of TeO_x structural units are well represented, including atypical environments in $BaTe_2O_6$ and $Cs_2Te_4O_{12}$ structures. In this paper we present the results concerning the pure TeO_2 polymorphs only. The detailed information for other structures is given in [30].

The comparison between calculated and experimental lattice parameters for $\alpha-$, $\beta-$ and $\gamma-TeO_2$ is reported in Table 2 and characteristic Te–O bond lengths and angles are listed in Table 3. One can point out that the general feature of the derived potentials is an underestimation of short Te–O bond lengths and a slight overestimation of intermediate Te–O bond lengths. In Table 3 we list the total bond-valences for each Te atom site calculated with Brown and Altermatt formulae [51] as well. As we can see, calculated values for optimised structures are overestimated because of the important contribution of the short bonds into the total atom bond-valence.

Let us now point out some subtle structural peculiarities of γ-TeO_2 polymorph which we managed to reproduce using our IAPs. This polymorph is especially interesting because it is considered as the crystalline structure closest to glass. Indeed, γ-TeO_2 polymorph crystallises first while heating the glass and the Raman spectra of glass has much more common bands with γ-TeO_2 than with α-TeO_2 or β-TeO_2 polymorphs [17]. As was discussed above, γ-TeO_2 is made of TeO_4E structural units with three short ($<$ 2.02 Å) Te–O bonds and one elongated bond (2.2 Å), which by sharing oxygen corners frame the three-dimensional network illustrated in Fig. 3. Such a network forms wide rectangular tunnels containing the LPs of tellurium atom [17]. Let us now compare the structure of γ-TeO_2 with that of the paratellurite, α-TeO_2 (Fig.4). In both structures basic units are interconnected via Te–O–Te bridges with the following difference: α-TeO_2 contains a unique type of bridges, which are essentially asymmetric (1.87–2.12 Å), whereas in γ-TeO_2, the TeO_4E units are alternately linked by both nearly symmetric (1.95–2.02 Å) and highly asymmetric (1.86–2.20 Å) bridges. According to Champarnaud *et al.* [17] the resemblance of the Raman spectra of γ-TeO_2 and that of glass comes from vibrations of symmetric Te–O–Te bridges; thus it appears that such bridges represent one of the main structural features of TeO_2 glasses. Although the errors in bond lengths exaggerate a bit the subtle difference in symmetric and asymmetric bridges in optimised structures, our IAPs model has a critical ability for distinction between TeO_4 and TeO_{3+1} units for successful application to glass simulation.

Table 2 Calculated and experimental lattice parameters for investigated structures

Parameter	Exp.	Calc.	Difference, %
α-TeO_2			
a, b, Å	4.810	4.831	-0.44
c, Å	7.613	7.349	3.46
Volume, Å^3	176.135	171.548	2.60
α, β, γ	90	90	0.0
β-TeO_2			
a, Å	12.035	11.550	4.03
b, Å	5.464	5.473	-0.17
c, Å	5.607	5.549	1.03
Volume, Å^3	368.712	350.814	4.85
α, β, γ	90	90	0.0
γ-TeO_2			
a, Å	4.898	5.084	-3.79
b, Å	8.576	8.312	3.08
c, Å	4.351	4.196	3.55
Volume, Å^3	182.765	177.326	2.98
α, β, γ	90	90	0.0

4 Molecular dynamics study of the TeO_2 glass structure

MD simulations were performed with the DL_POLY [53] code. The core-shell model requires a special treatment in MD simulations. In this work, the relaxed shell model [54] implemented in DL_POLY was used. With this method, the massless shell is firstly relaxed before integration of the atomic motion and then the motion of the finite mass core is integrated by con-

This journal is © The Royal Society of Chemistry [year]

Physical Chemistry Chemical Physics Accepted Manuscript

Table 3 Bond lengths, angles (only for α,γ-TeO_2), bond-valences for each tellurium site and value of Te and O shells displacements (x_{Te} and x_O) according to corresponding cores for experimental and optimised structures

Bond	Exp., Å	Calc., Å	Difference, %	V^*_{exp}	V^*_{calc}	Difference, %	x_{Te}, Å	x^{**}_O, Å
α-TeO_2								
Te–$O_{1,2}$	1.880	1.836	2.31	4.06	4.32	-6.39	0.504	0.182
Te–$O_{3,4}$	2.121	2.130	-0.42					
Angles, °								
O_1–Te–O_2	103.343	110.449	-6.87					
O_3–Te–O_4	167.938	174.492	-3.90					
β-TeO_2								
Te–O	1.877	1.836	2.18	3.93	4.20	-6.95	0.501	0.194
Te–O	1.927	1.886	2.13					
Te–O	2.070	2.025	2.17					
Te–O	2.196	2.299	-4.69					
γ-TeO_2								
Te–O_1	1.859	1.819	2.15	3.99	4.27	-7.20	0.525	0.199
Te–O_2	1.948	1.865	4.26					
Te–O^1_1	2.197	2.253	-2.55					
Te–O^2_1	2.019	2.060	-2.03					
Angles, °								
O_1–Te–O_2	99.2	102.176	-3.00					
O^1_1–Te–O^2_1	153.6	147.884	3.72					

**Bond-valences are calculated using re-determined bond-valence parameters for* Te^{4+} – O*:* $r_0 = 1.9605Å, b = 0.41$ [52] *and neighbours out to 3.5 Å were included*

***Core/shell distances for O atoms are averaged over all oxygen sites in the structure*

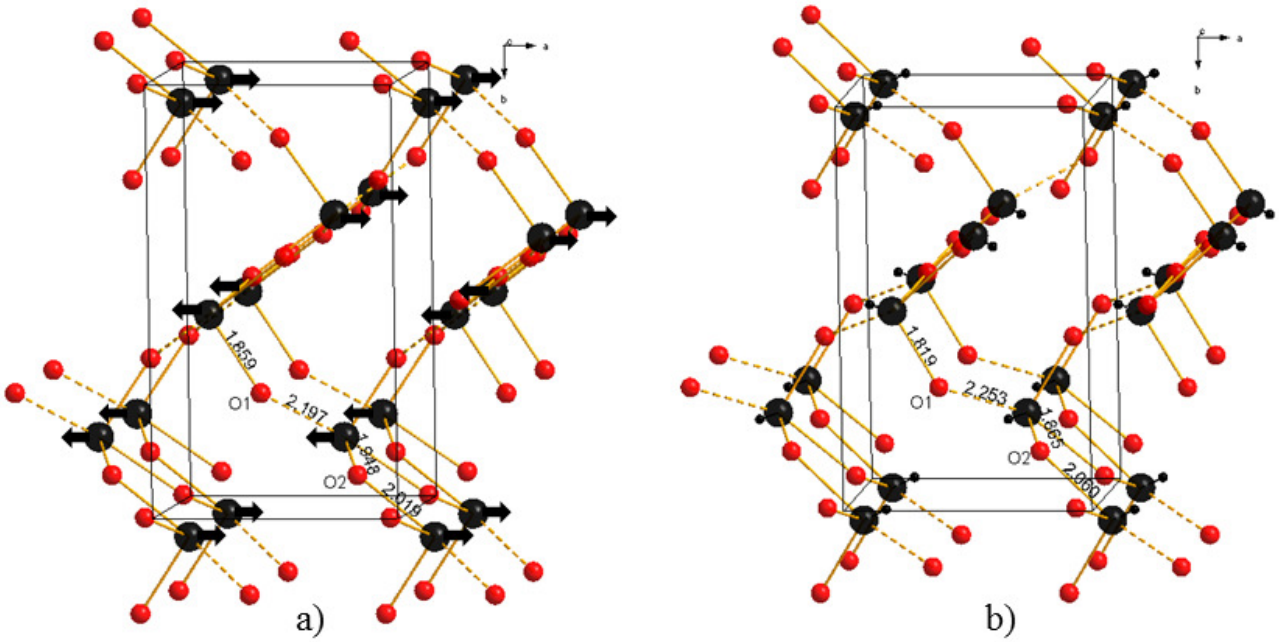

Fig. 3 (Color online) Spatial view of γ-TeO_2 structure: a) Experimental structure and b) Optimised structure. The notations for bonds and atoms are the same as in Fig. 1, in a) the arrows indicate the direction of the Te LP and in b) the small black circles correspond to the Te shell optimised coordinates. The bond lengths are in Å.

Physical Chemistry Chemical Physics Accepted Manuscript

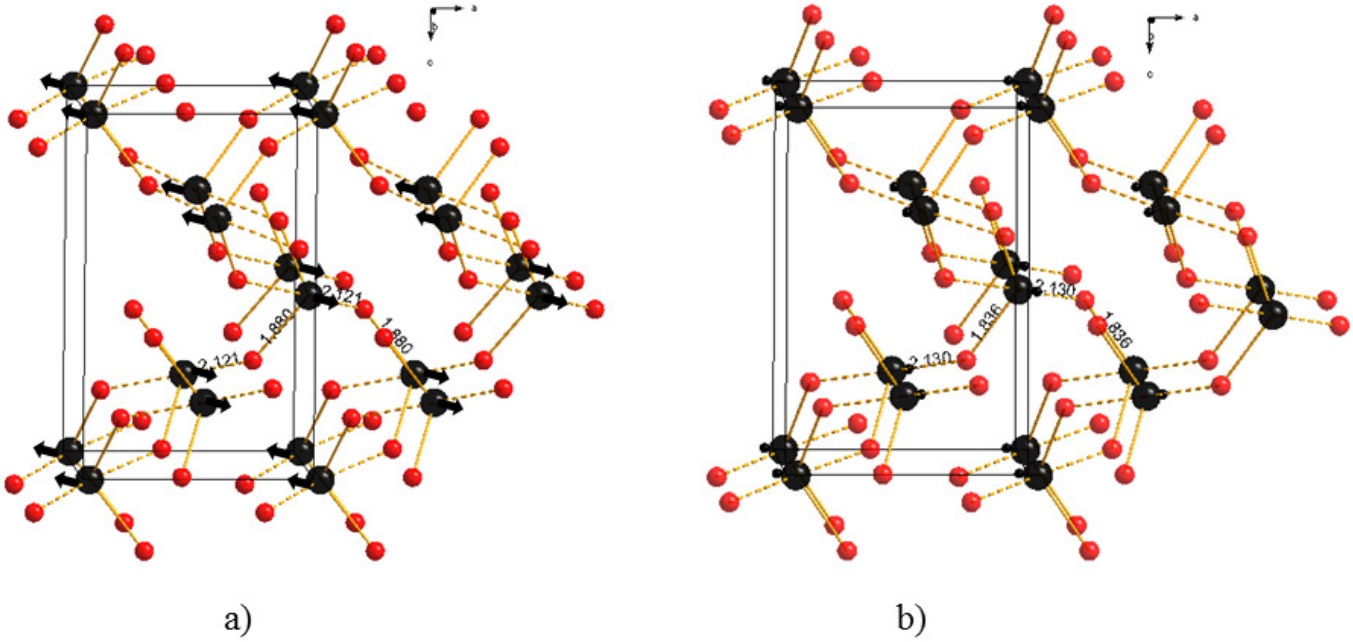

Fig. 4 (Color online) Spatial view of α-TeO_2 structure: a) Experimental structure and b) Optimised structure. The notations for bonds and atoms are the same as in Fig. 1, in a) the arrows indicate the direction of the Te LP and in b) the small black circles correspond to the Te shell optimised coordinates. The bond lengths are in Å.

ventional MD.

The final model of the pure TeO_2 glass was obtained starting from the draft glass model obtained after test runs. The simulation box (31.76 Å×34.62 Å×30.58 Å) contained 4032 particles (= 2016 cores and 2016 shells). We used the NPT ensemble and a time step of 1.0 fs for integration of the equations of motion. Firstly, the system was heated up to 2050 K (the γ-TeO_2 melting temperature according to the test runs) and kept for about 150 ps following which it was cooled down to 1000 K and kept for about 70 ps more, and after is was cooled down to 500 K and kept at this temperature for about 70 ps more. Then, the system was cooled down to 300 K and kept at this temperature for about 50 ps. Unfortunately, it was not possible to use the shell model for both Te and O atoms (*i.e.* with harmonic spring potential interaction for O(core)–O(shell) system and quartic spring potential interaction for Te(core)–Te(shell) system) during this quenching procedure. Indeed, despite the fact that the shell relaxation was very time-consuming, frequent and random abortions of the simulation occurred because of convergence problem of the shell relaxation algorithm in DL_POLY. Consequently, we used the rigid-ion model for oxygen atoms during the quenching procedure and the full shell model was only used for annealing the system at 300 K during about 20 ps in order to obtain the final configuration. The fact that the shell model for oxygen atoms was not activated when the atomic diffusion is high may induce defects in the medium range-order of the glass model (as discussed in Sec. 6). The temperature variation as a function of time is shown in Fig. 5 and corresponds to $5.4{\cdot}10^{12}$ K/s cooling rate in average. The atomic density of the modelled glass structure is 0.0626 at/Å^3.

5 Experimental PDF

The pure TeO_2 glass sample was synthesised starting from orthotelluric acid H_6TeO_6 (Aldrich 99.9%). Orthotelluric acid was first thermally decomposed at 550°C for 24 hours in order to obtain powdered $\alpha-TeO_2$. The powder was then put in a platinum crucible and melted at 800°C for 30 minutes and finally quenched using a mixture of water, NaCl and ethanol at about -10 °C. As only a small quantity of glass (few decigrams) was obtained after each synthesis, this procedure was repeated in order to obtain a few grams. The measured density of the sample is ρ_{exp} = 5.57 g/cm^3, which corresponds to a atomic density 0.063 at/Å^3.

The experimental PDF was obtained thanks to a neutron total scattering experiment carried out at the 7C2 diffractometer of the LLB (Laboratoire Lèon Brillouin), Saclay, France. The used wavelength of 0.701 Å enabled us to record intensities up to $Q_{max} = 16\text{Å}^{-1}$ ($Q = 4\pi sin\theta/\lambda$). The powder samples were

This journal is © The Royal Society of Chemistry [year]

Physical Chemistry Chemical Physics Accepted Manuscript

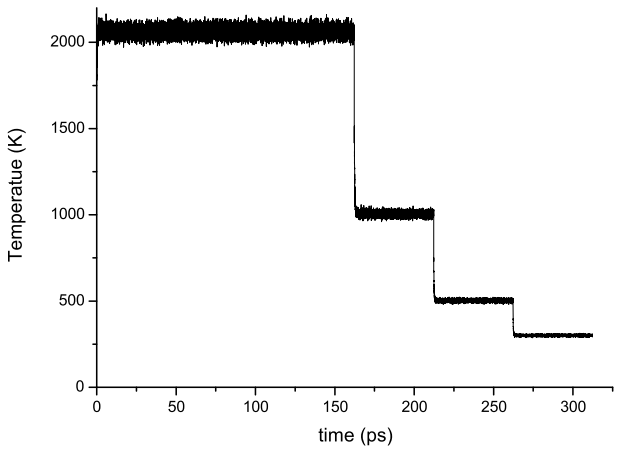

Fig. 5 Temperature as a function of time in the TeO_2 glass preparation procedure.

placed in a thin-walled (2.5 micrometers) vanadium container of 6 mm in diameter. The experiment was performed under vacuum at room temperatures. Raw data were corrected for empty cell, absorption, inelastic and multiple scattering and normalised using the program CORRECT[55]. The total PDF was then derived from the structure factor using the MCGR program[56]. This Monte Carlo-based inversion method allows in contrast to the conventional direct Fourier transform, to correctly handle noise, truncation of data and the finite resolution of the instrument.

6 Results

6.1 Pair distribution functions

In Fig. 6 we report the calculated total distribution function $T(r)$ together with the experimental one. The envelope of calculated $T(r)$ is in good agreement with the experimental one, which let us conclude that the modelled glass structure is consistent with the real one. The first peak of the calculated $T(r)$ corresponds to the shortest Te–O distances and is slightly shifted to smaller r values with respect to the experimental data. This accords with the underestimation of the Te–O bond lengths found with the crystalline structures optimised with our IAPs . Also it shows a more explicit shoulder at ≈ 2.13 Å than the experimental $T(r)$, which is attributed to elongated axial Te–O bonds. The second peak shows a more significant inaccuracy in calculated $T(r)$. This peak has the main contribution from the O–O partial distribution function (see Fig. 7) and is shifted to the larger r values (2.83 Å) with respect to the experimental one (2.77 Å). It implies that in our model the O–O distances are slightly exaggerated, but this does not effect a lot neither Te atom coordination, nor TeO_x units interconnection. The third peak at 3.47 Å is very representative for TeO_x units interconnections, as it corresponds to the shortest Te–Te distances, and it fits very well the experimental data. The most important disagreement between calculated and experimental $T(r)$ is in the fourth peak position. The calculated value is 4.40 Å and corresponding experimental value is 4.67 Å. As we can see in Fig. 7, all three partial PDFs contribute to this peak to a large extent, so that it is difficult to define the origin of this error. Possibly, this error is due to the use of the rigid-ion model for oxygen atoms during the quenching process.

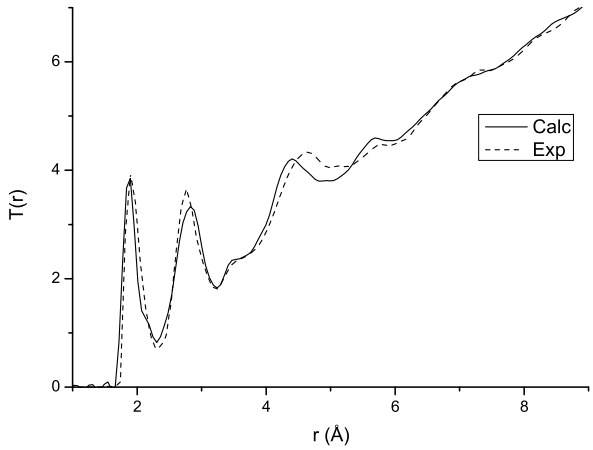

Fig. 6 Total distribution function obtained with MD simulations (solid line) and compared with the neutron diffraction data (dotted line).

Fig. 7 shows all the partial PDFs, which have no oscillations in the region for $r > 9$ Å. This indicates an appropriate choice of the simulation box size. The Te–O partial PDF has a sharp first peak with the maximum at 1.865 Å and a broad asymmetric shoulder up to the first minimum at 2.46 Å. The average coordination numbers of Te and O atoms (n_{TeO} and n_{OTe}) calculated by integrating $T_{TeO}(r) = 4\pi r^2 \rho G_{TeO}(r)$ with cutoff radius R_{cutoff} = 2.46 Å have values of 3.93 and 1.97 respectively. These values are lower than those in crystalline structures (4 and 2). They are also in a good agreement with the *ab initio* MD results of Pietrucci *et al.* ($n_{TeO} = 3.69$ and $n_{OTe} = 1.85$) and with experimental results of Barney *et al.* ($n_{TeO} = 3.68(4)$ and $n_{OTe} = 1.84(1)$) obtained with total neutron scattering techniques. In these works, a cutoff radius of 2.36 Å (proposed in[10] as well) was used. If we now calculate the coordination numbers with this cutoff value, we obtain $n_{TeO} = 3.73$ for tellurium atom and $n_{OTe} = 1.86$ for oxygen

Physical Chemistry Chemical Physics Accepted Manuscript

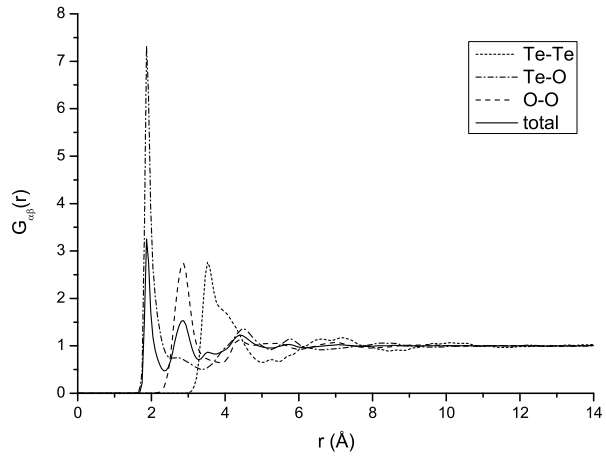

Fig. 7 Partial and total radial pair distribution functions for modelled TeO_2 glass.

atom, which are in better agreement with the literature. As we can see, the Te atoms coordination number in tellurites is very sensitive to R_{cutoff} value and we will develop a detailed discussion on this problem in the next section.

6.2 Tellurium coordination number

Let us now discuss in more details the problem of tellurium coordination number and cutoff radius for Te–O bonds. Fig. 8 (solid line) shows coordination number of Te atoms as a function of the cutoff radius. The coordination number curve keeps increasing without any flat region indicating a large variety of Te–O distances. This means that there is no characteristic cutoff radius that could unambiguously define the first coordination sphere of tellurium atom and its coordination number. This problem of the broad Te–O distances distribution and no univocal definition of cutoff radius was already raised in [18,21], but it has never been considered more elaborately. In this work we propose to explicitly take into account the presence of the Te LP, when defining the cutoff radius for Te–O bonds. Each TeO_x unit has its stereo-chemically active Te LP on one side and the bonded oxygen atoms on the other side. So it is incorrect to consider oxygen atoms on the LP side as being bonded to the Te atoms even if they lie within the given cutoff radius.

The explicit treatment of tellurium LP as a shell allows us to distinguish between bonded and non-bonded oxygen atoms in the Te coordination sphere of given radius. For this purpose we considered the distribution of the angles (ϕ) between oxygen atom inside the Te coordination sphere of the radius $R_{cutoff} = 2.46$ Å, Te core and Te shell (the LP) (Fig. 9). As we can see, this distribution consists of three regions: two broad peaks at 80–100 degrees and at 110–140 degrees which correspond to axial and equatorial oxygen atoms respectively, and a shoulder between 50 and 80 degrees on the left. This last interval corresponds to the oxygen atoms that lie on the LP side of the TeO_x unit and should not be taken into account when calculating Te coordination number.

We investigated Te atom environment in a number of crystalline tellurite structures and defined a new criterion $\phi_{cutoff} = 75^\circ$ for oxygen atoms that contribute to Te coordination number. The dotted line in Fig. 8 shows a new accumulated coordination number for Te–O pairs considering the new cutoff criterion and this time the curve has a characteristic flat region that starts from approximately 2.4 Å. Now when calculating the coordination numbers of Te and O atoms from the glass structure configuration and taking into account two cutoff criteria $\phi_{cutoff} = 75^\circ$ and $R_{cutoff} = 2.46$ Å, we obtain $n_{TeO} = 3.63$ and $n_{OTe} = 1.81$. These values are clearly smaller than those obtained with the same cutoff radius but without the ϕ_{cutoff} criterion. This indicates that not taking into account this latter criterion systematically overestimates the coordination number by including incorrect oxygen atoms from a chemical point of view. In addition, using $R_{cutoff} = 2.36$ Å and $\phi_{cutoff} = 75^\circ$ does not change so much the coordination numbers ($n_{TeO} = 3.55$ and $n_{OTe} = 1.77$), which confirms the robustness of the ϕ criterion. From these remarks it appears that for tellurite glass systems, the first minimum of the $T_{TeO}(r)$ (2.46 Å) is not the best choice for calculating the coordination number, and that a smaller cutoff radius value (for example, 2.36 Å) gives a better estimation if the ϕ_{cutoff} criterion is not considered.

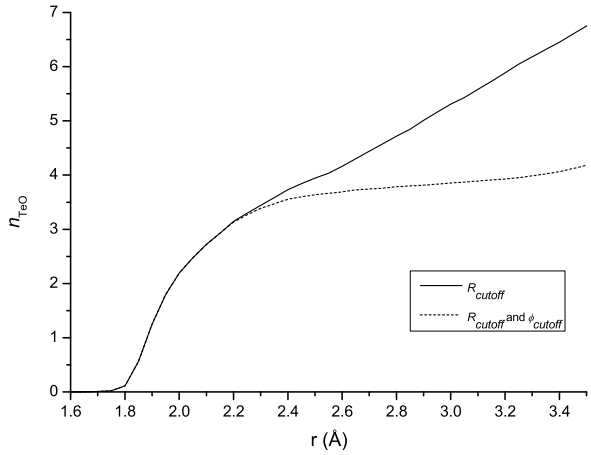

Fig. 8 Accumulated tellurium atom coordination number with only R_{cutoff} criterion (solid line) and with two cutoff criteria $\phi_{cutoff} = 75^\circ$ and R_{cutoff} (dotted line).

Physical Chemistry Chemical Physics Accepted Manuscript

This journal is © The Royal Society of Chemistry [year]

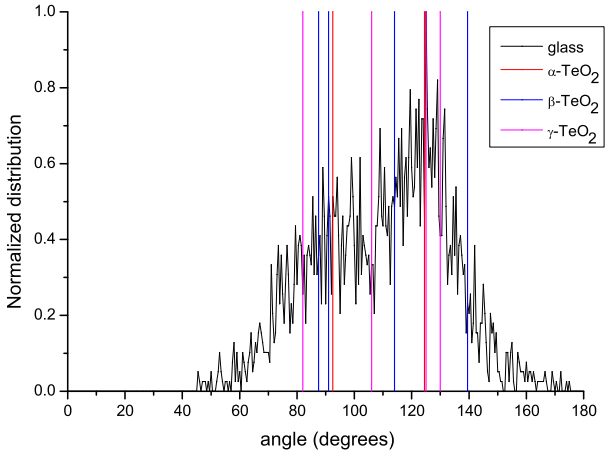

Fig. 9 (Color online) Normalised O–Te(core)–Te(shell) angle distribution glass within $R_{cutoff} = 2.46$ Å in TeO_2 glass model. Color vertical lines correspond to these angles in α- (red), β- (blue) and γ-TeO_2 (magenta) crystalline structures (optimised with used IAP).

terion.

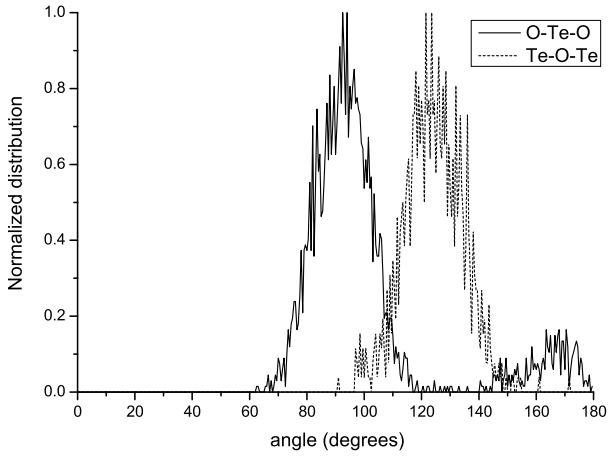

Fig. 10 Normalised BAD. The solid line is for O–Te–O BAD and the dashed line is for Te–O–Te BAD.

6.3 Structural units distribution

The structural units distribution of the glass structure model obtained with the best criteria ($R_{cutoff} = 2.46$ Å and $\phi_{cutoff} = 75°$) are reported in Table 4. It shows that the structure contains a large variety of Q^n_m polyhedra with a large proportion (about 43%) of threefold units. This directly contributes to the decrease of Te coordination number to $n_{TeO} = 3.63$. There is about 50% of four-coordinated Te atoms and a small amount (7%) of five-coordinated Te atoms. A large content (21%) of terminal oxygen atoms bonded only to one Te atom was found in the glass structure and a negligible amount (about 3%) of three-coordinated oxygen atoms.

In Table 4 we also give the Q^n_m polyhedra distribution calculated with other cutoff values discussed in previous section. As we can see, considering the $R_{cutoff} = 2.46$ Å without ϕ cutoff criterion gives the highest discrepancies, which emphasises the discussion of Sec. 6.2.

The O–Te–O and Te–O–Te bond-angle distributions (BAD) are reported in Fig. 10. The O–Te–O BAD has two peaks: one between 70°– 110°and the other, much less intense, between 150°– 180°. The peak at smaller angles includes the O_{eq}–Te–O_{eq} angles of $\alpha-$, $\beta-$ and $\gamma-TeO_2$ phases (99°– 103°), but its maximum is shifted to 90° that corresponds more to TeO_3 pyramidal units. The second peak corresponds to O_{ax}–Te–O_{ax} angles. A quite narrow peak of Te–O–Te BAD argues for rather corner-sharing character of polyhedra connection and the absence of edge-sharing polyhedra. The BAD statistics does not differ significantly when considering only R_{cutoff} cri-

6.4 Rings statistics

In order to obtain the information on the Intermediate Range Order (IRO) of the glass, we performed the rings statistics analysis of the final MD configuration. We used the RINGS code[57] for this purpose. RINGS allows obtaining the following quantities: $R_C(n)$, the number of rings of n nodes per cell in the material, $P_N(n)$, the proportion of nodes, which form at least one ring of size n, and the probabilities $P_{max}(n)$ and $P_{min}(n)$, that a ring with n nodes represents respectively the longest or the shortest ring for given node[57]. A n-membered ring is a ring containing n nodes and the results are reduced to the total number of nodes in the networks. In such a manner, it is possible to compare the results for systems with different number and/or nature of nodes.

In Fig. 12 we present the rings statistics of the final MD configuration obtained for primitive rings search. A ring is primitive[58] if it can not be decomposed into two smaller rings. It is significant, that for rings statistics analysis with RINGS we could use only $R_{cutoff} = 2.36$ Å criterion, but we suppose that consideration of the ϕ_{cutoff} criterion would have changed quantitative results not very strongly, while qualitative conclusions would have rested the same. The rings analysis was carried out using 30 nodes as maximum search depth.

The $R_C(n)$ values for TeO_2 system are really low, which indicates the small amount of rings in the system and hence the weak network connectivity. Furthermore, the rings with $n \geq 10$ predominate in the TeO_2 glass configuration. As $P_N(n)$, the proportion of nodes, is high for rings with $n \geq 10$, they can

Physical Chemistry Chemical Physics Accepted Manuscript

Table 4 The Q_m^n units distribution in % in the TeO_2 modelled glass structure.

	Q_3^1	Q_3^2	Q_3^3	Q_4^2	Q_4^3	Q_4^4	Q_5^4	Q_5^5
This work (ϕ_{cutoff} and $R_{cutoff} = 2.46$ Å)	1.19	18.15	23.96	0.59	19.05	30.51	2.08	4.46
This work ($R_{cutoff} = 2.46$ Å)	0.0	4.76	20.68	0.29	10.27	46.13	3.27	13.99
This work (ϕ_{cutoff} and $R_{cutoff} = 2.36$ Å)	1.49	22.17	26.04	0.74	18.75	25.06	2.08	3.13
This work ($R_{cutoff} = 2.36$ Å)	0.45	12.8	24.4	0.59	14.29	37.95	2.83	6.55
Ab initio MD [18]	0.6	14.9	20.4	0	17.1	35.9	0	9.4

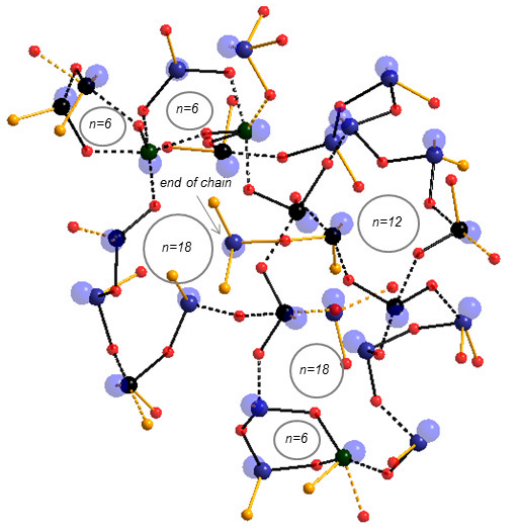

Fig. 11 (Color online) Fragment of pure TeO_2 glass structure obtained with MD simulations with found rings. Oxygen atoms are presented in the small spheres (red for BO and yellow for NBO), tellurium atoms are the medium size spheres (black for four-coordinated, indigo for three-coordinated and dark green for five-coordinated Te) and Te LPs are the big transparent blue spheres. The solid lines represent the short Te–O bonds (< 2.02 Å) and dashed lines represent intermediate and long bonds ($2.02 < d < 2.36$ Å). The black bonds emphasise the rings in the structure and n in the circles indicates the amount of nodes in each found ring.

be considered as a global characteristic of the network.

Let us now consider the $P_{min}(n)$ and $P_{max}(n)$ values. For $n < 8$ we get $P_{min}(n) \cong 1$ meaning that the small rings of 4–8 nodes are always the shortest path for the given node and, hence, one particular node can not be the origin of several small rings. Otherwise it would be an evidence for a quite compact glass structure. The $P_{max}(n)$ reaches the value of 1 only for 30 nodes search. This implies, that the shortest paths of 30 nodes could be found and points out on the openness of the network and the presence of voids in the structure.

7 Discussion

Having done the statistics description of the glass structure let us consider a random fragment of the modelled glass structure. In Fig. 11 several rings are presented as well as chains with terminal oxygen (NBO) atoms. TeO_x units tend to form large rings ($n \geq 10$), probably, because of the tellurium LP (big blue transparent spheres in Fig. 11) steric effect. When forming small rings, each TeO_x unit should take into account its orientation with respect to the other, because all the LPs could not be oriented inside the small ring. Accordingly, they are the reason of forming such an open network with voids created by the LP steric effect. The network connectivity computed directly, as the average number of bridging oxygen atoms bound to each tellurium atom, is equal to 3.2.

From the rings statistics and from. Fig. 11 we can see that a large amount of NBO atoms (see Sec. 6.3) in the glass structure plays an important role (together with electronic LP steric effect) in forming the glass network. This could be due to the high proportion of terminal oxygen atoms that prevents the closure of the rings and indicates a more open network [59].

Our model of the amorphous TeO_2 structure agrees in general with the one proposed in [20], but it is much more irregular and consists of a larger variety of TeO_x units. Indeed, our model of open network with weak connectivity and a large amount of terminal oxygen atoms supports the concept that NBO atoms and low tellurium coordination numbers are the reason of facile accommodation of modifier atoms, as expressed in [20]. Possibly, the surplus of NBO atoms allows stabilising the glass structure when adding a modifier (M_nO_m) by creating M–O bongs with terminal oxygen atoms thus reinforcing the connectivity of the glass network.

Let us now compare our amorphous TeO_2 model with one obtained by *ab initio* MD simulations in [18]. The Q_m^n structural units distribution in that work is quite close to those for our model (particularly if considering only R_{cutoff} criterion). Pietrucci *et al.* report about 14% of NBO atoms which is 7% less than in our model. As mentioned above, the authors suppose that such a large concentration of NBO atoms is due to a

This journal is © The Royal Society of Chemistry [year]

Physical Chemistry Chemical Physics Accepted Manuscript

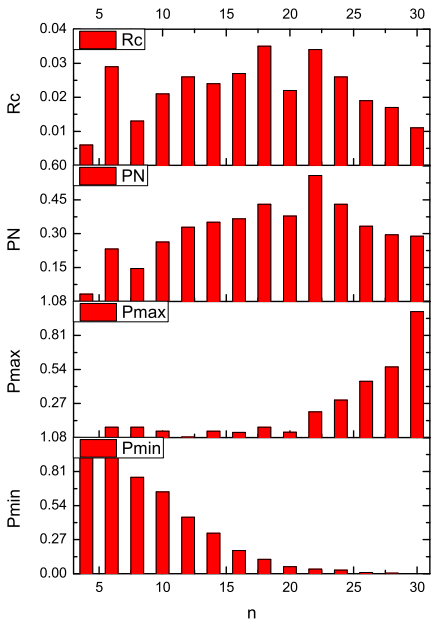

Fig. 12 Primitive rings statistics for pure TeO_2 modelled glass. $R_C(n)$ is the number of rings of n nodes per cell in the material, $P_N(n)$ is the proportion of nodes, which form at least one ring of size n, and $P_{max}(n)$ and $P_{min}(n)$ are the probabilities, that a ring with n nodes represents respectively the longest or the shortest ring for given node.

high cooling rate used in the quenching protocol, which might have brought the system to the frozen liquid state. The glass model in their work was obtained as a result of 16 ps cooling the liquid at a rate of $\cong 10^{14}$ K/s, as *ab initio* simulations are very time-consuming. With our classical MD simulations, we could perform a much longer quenching protocol. As it was mentioned in Sec. 4, the total simulated time is about 350 ps which is significantly longer. Nevertheless, we found even more NBO atoms and weaker connectivity of the network as in *ab initio* MD simulated glass structure. Thus we suppose that these are really characteristics of the TeO_2 amorphous state.

8 Conclusions

We have presented for the first time IAPs for TeO_2-based systems and their application to the study of pure amorphous TeO_2 by MD simulations. The potential model is simple but has some nontrivial features: the short-range interatomic interaction in the core-shell model frameworks is set between the Te atom core and O atom shell and the core-shell model for Te atom uses an anharmonic spring potential form. This approach is reported for the first time in the literature and works well for different TeO_2-based compounds.

The derived potential successfully reproduces the structure of all the pure TeO_2 polymorphs and a number of mixed TeO_2-based compounds, and the various Te atom coordinations. The subtle difference between Q_4^4 polyhedron in $\alpha-TeO_2$ and Q_{3+1}^4 polyhedron in $\gamma-TeO_2$ is well represented that is evidence for a good quality of IAPs appropriate for MD simulation glass modelling.

MD simulation of the pure TeO_2 glass was performed for a system containing 672 TeO_2 units and a total simulation time of about 350 ps. The calculated total PDF is in a good agreement with the experimental one obtained by neutron diffraction method. Hence we consider our glass structure model as realistic.

The glass structure model has a broad Q_m^n units distribution with a large variations of Te–O bond lengths. We developed a new criterion that allows to precisely define the first coordination sphere of Te atom by explicitly taking into account the Te stereochemically active electronic LP. This criterion is the angle between oxygen atom inside the Te coordination sphere of the radius $R_{cutoff} = 2.46$ Å, Te core and Te shell (the LP) and it was set to 75°.

The Te coordination number in the modelled glass is $n_{TeO} = 3.63$ and is in good agreement with these ones obtained by *ab initio* MD simulation [18] and by neutron diffraction methods [20]. This result together with Q_m^n units distribution implies a large amount of NBO (21%) in the glass structure, which confirms the results of the mentioned above studies as well.

We carried out the rings statistics analysis and investigated the modelled glass structure. The pure amorphous TeO_2 network has a weak connectivity, terminated chains and large ($n \geq 10$) rings. This is due to large number of NBO and stereochemical effect of Te electronic LP that the TeO_2 glass has such a badly connected network. Possibly, these peculiarities explain the instability of the glass towards to devitrification and its good ability to accommodate the modifiers.

Acknowledgments

We would like to thank the Laboratoire Léon Brillouin (LLB), Saclay, France for providing neutron beam time and the LLB staff, in particular B. Beuneu, for experimental support.

References

1 R. A. El-Mallawany, *Tellurite glasses handbook: physical properties and data*, CRC Press, Second edition edn., 2012.

2 S. Suehara, P. Thomas, A. P. Mirgorodsky, T. Merle-Méjean, J. C. Champarnaud-Mesjard, T. Aizawa, S. Hishita, S. Todoroki, T. Konishi and S. Inoue, *Phys. Rev. B*, 2004, **70**, 205121.

3 A. P. Mirgorodsky, M. Soulis, P. Thomas, T. Merle-Méjean and M. Smirnov, *Phys. Rev. B*, 2006, **73**, 134206.

Physical Chemistry Chemical Physics Accepted Manuscript

4 M. Soulis, T. Merle-Mejean, A. Mirgorodski, O. Masson, E. Orhan, P. Thomas and M. Smirnov, *Journal of Non-Crystalline Solids*, 2008, **354**, 199–202.

5 M. Smirnov, A. Mirgorodsky, O. Masson and P. Thomas, *The Journal of Physical Chemistry A*, 2012, **116**, 9361–9369.

6 T. Sekiya, N. Mochida, A. Ohtsuka and M. Tonokawa, *Journal of non-crystalline solids*, 1992, **144**, 128–144.

7 A. Mirgorodsky, M. Colas, M. Smirnov, T. Merle-Mjean, R. El-Mallawany and P. Thomas, *Journal of Solid State Chemistry*, 2012, **190**, 45 – 51.

8 S. Sakida, S. Hayakawa and T. Yoko, *Journal of non-crystalline solids*, 1999, **243**, 1–12.

9 S. Sakida, S. Hayakawa and T. Yoko, *Journal of non-crystalline solids*, 1999, **243**, 13–25.

10 J. C. McLaughlin, S. L. Tagg, J. W. Zwanziger, D. R. Haeffner and S. D. Shastri, *Journal of Non-Crystalline Solids*, 2000, **274**, 1–8.

11 J. C. McLaughlin, S. L. Tagg and J. W. Zwanziger, *The Journal of Physical Chemistry B*, 2001, **105**, 67–75.

12 J. W. Zwanziger, J. C. McLaughlin and S. L. Tagg, *Physical Review B - Condensed Matter and Materials Physics*, 1997, **56**, 5243–5249.

13 U. Hoppe, I. Gugov, H. Brger, P. Jvri and A. Hannon, *Journal of Physics Condensed Matter*, 2005, **17**, 2365–2386.

14 I. P. Kondratyuk, L. A. Murdoyan, Y. V. Pisarevskij and V. I. Simonov, *Kristallografiya*, 1987, **32**, 609–617.

15 P. A. Thomas, *Journal of Physics C: Solid State Physics*, 1988, **21**, 4611.

16 H. Beyer, *Zeitschrift für Kristallographie*, 1967, **124**, 228–237.

17 J. Champarnaud-Mesjard, S. Blanchandin, P. Thomas, A. Mirgorodsky, T. Merle-Mejean and B. Frit, *Journal of Physics and Chemistry of Solids*, 2000, **61**, 1499 – 1507.

18 F. Pietrucci, S. Caravati and M. Bernasconi, *Phys. Rev. B*, 2008, **78**, 064203.

19 W. H. Zachariasen, *Journal of the American Chemical Society*, 1932, **54**, 3841–3851.

20 E. R. Barney, A. C. Hannon, D. Holland, N. Umesaki, M. Tatsumisago, R. G. Orman and S. Feller, *The Journal of Physical Chemistry Letters*, 2013, 2312–2316.

21 H. Matsumoto, T. Mabuchi, Y. Shigesato and I. Yasui, *Japanese Journal of Applied Physics*, 1996, **35**, 694–698.

22 B. G. Dick and A. W. Overhauser, *Phys. Rev.*, 1958, **112**, 90–103.

23 C. R. A. Catlow, R. James, W. C. Mackrodt and R. F. Stewart, *Physical Review B (Condensed Matter)*, 1982, **25**, 1006–1026.

24 C. M. Freeman and C. R. A. Catlow, *Journal of Solid State Chemistry*, 1990, **85**, 65 – 75.

25 J. D. Gale, *The General Utility Lattice Program v.3.1 Users Manual*, http://projects.ivec.org/gulp/help/manuals.html.

26 J. D. Gale, *J. Chem. Soc., Faraday Trans.*, 1997, **93**, 629–637.

27 H. Ogi, M. Fukunaga, M. Hirao and H. Ledbetter, *Phys. Rev. B*, 2004, **69**, 024104.

28 Q.-J. Liu, Z.-T. Liu, L.-P. Feng and H. Tian, *Physica B: Condensed Matter*, 2010, **405**, 3159 – 3163.

29 http://www.ucl.ac.uk/klmc/Potentials/Library/catlow.lib.

30 A. Gulenko, O. Masson, A. Berghout, D. Hamani and P. Thomas, *To be published*, 2014, 00–00.

31 M. C. Wojcik and K. Hermansson, *Chemical Physics Letters*, 1998, **289**, 211 – 218.

32 M. Sepliarsky, Z. Wu, A. Asthagiri and R. Cohen, *Ferroelectrics*, 2004, **301**, 55–59.

33 J. M. Vielma and G. Schneider, *Journal of Applied Physics*, 2013, **114**, 174108.

34 M. Sepliarsky, A. Asthagiri, S. Phillpot, M. Stachiotti and R. Migoni, *Current Opinion in Solid State and Materials Science*, 2005, **9**, 107 – 113.

35 F. Folger, *Zeitschrift fuer Anorganische und Allgemeine Chemie*, 1975, **411**, 103–110.

36 R. Masse, J. Guitel and I. Tordjman, *Materials Research Bulletin*, 1980, **15**, 431–436.

37 L. Andersen, V. Langer, A. Stromberg and D. Stromberg, *Acta Crystallographica Section B: Structural Science*, 1989, **45**, 344–348.

38 B. Loopstra and K. Goubitz, *Acta Crystallographica Section C: Crystal Structure Communications*, 1986, **42**, 520–523.

39 M. Weil, *Acta Crystallographica Section E: Structure Reports Online*, 2005, **61**, i237–i239.

40 W. Klein, J. Curda, E.-M. Peters and M. Jansen, *Zeitschrift für anorganische und allgemeine Chemie*, 2005, **631**, 2893–2899.

41 M. Kocak, C. Platte and M. Troemel, *Acta Crystallographica*, 1979, **B35(6)**, 1439–1441.

42 H. Rossell, M. Leblanc, G. Ferey, D. Bevan, D. Simpson and M. Taylor, *Australian Journal of Chemistry*, 1992, **45**, 1415–1425.

43 M. Weil and B. Stoger, *Acta Crystallographica Section C: Crystal Structure Communications*, 2008, **64**, i79–i81.

44 V. M. Trömel and T. Scheller, *Zeitschrift für anorganische und allgemeine Chemie*, 1976, **427**, 229–234.

45 T. Siritanon, J. Li, J. K. Stalick, R. T. Macaluso, A. W. Sleight and M. Subramanian, *Inorganic chemistry*, 2011, **50**, 8494–8501.

46 F. Daniel, J. Moret, M. Maurin and E. Philippot, *Acta Crystallographica Section B*, 1978, **34**, 1782–1786.

47 S. Tagg, J. Huffman and J. Zwanziger, *Chemistry of materials*, 1994, **6**, 1884–1889.

48 C. Platte and M. Tromel, *Acta Crystallographica Section B: Structural Crystallography and Crystal Chemistry*, 1981, **37**, 1276–1278.

49 H. Mayer and M. Weil, *Zeitschrift fur Anorganische und Allgemeine Chemie*, 2003, **629**, 1068–1072.

50 N. Barrier, S. Malo, O. Hernandez, M. Hervieu and B. Raveau, *Journal of Solid State Chemistry*, 2006, **179**, 3484–3488.

51 I. Brown and D. Altermatt, *Acta Crystallographica Section B: Structural Science*, 1985, **41**, 244–247.

52 S. Mills and A. Christy, *Structural Science*, 2013, **69**, 145–149.

53 I. T. Todorov, W. Smith, K. Trachenko and M. T. Dove, *Journal of Materials Chemistry*, 2006, **16**, 1911–1918.

54 P. J. D. Lindan and M. J. Gillan, *Journal of Physics: Condensed Matter*, 1993, **5**, 1019.

55 M. Howe, R. McGreevy and P. Zetterström, *NFL Studsvik internal report*, 1996.

56 L. Pusztai and R. McGreevy, *Physica B: Condensed Matter*, 1997, **234**, 357–358.

57 S. L. Roux and P. Jund, *Computational Materials Science*, 2010, **49**, 70 – 83.

58 D. S. Franzblau, *Phys. Rev. B*, 1991, **44**, 4925–4930.

59 L. Cormier, D. Ghaleb, D. R. Neuville, J.-M. Delaye and G. Calas, *Journal of non-crystalline solids*, 2003, **332**, 255–270.

This journal is © The Royal Society of Chemistry [year]

Physical Chemistry Chemical Physics Accepted Manuscript

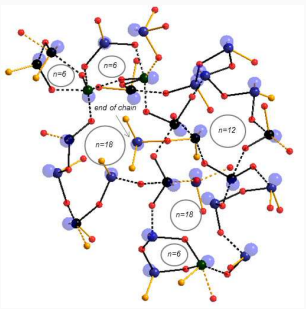

This article derives the interatomic potential for TeO_2 system and presents the first results of molecular dynamics simulations of pure TeO_2 structure.

Physical Chemistry Chemical Physics Accepted Manuscript